Synthesis and Characterization of Polyaniline/Carbon Nanotube Composites

S. Ghatak,[1] G. Chakraborty,[1] A. K. Meikap,[1] T. Woods,[2] R. Babu,[2] W. J. Blau[2]

[1]*Department of Physics, National Institute of Technology, Durgapur, Mahatma Gandhi Avenue, Durgapur 713 209, West Bengal, India*
[2]*Physics Department, University of Dublin, Trinity College, Dublin 2, Ireland*

Received 6 August 2009; accepted 10 December 2009
DOI 10.1002/app.31962
Published online 30 July 2010 in Wiley Online Library (wileyonlinelibrary.com).

ABSTRACT: The synthesis of polyaniline (PANI) containing different carbon nanotubes (CNTs) by *in situ* polymerization is reported in this study. The samples were characterized by X-ray diffraction and scanning electron microscopy. Fourier transform infrared and ultraviolet–visible spectroscopy were used to determine the change in structure of the polymer/CNT composites. Thermogravimetric analysis showed that the composites had better thermal stability than the pure PANI. Photoluminescence spectra showed a blueshift in the PANI–single-walled nanotube (SWNT) composite. Low-temperature (77–300 K) electrical transport properties were measured in the absence and presence of a magnetic field up to 1 T. Direct-current conductivity exhibited a nonohmic, three-dimensional variable range hopping mechanism. The room-temperature magnetoconductivity of all of the investigated samples except the PANI–SWNT composite were negative; however, it was positive for the PANI–SWNT composite, and its magnitude decreased with increasing temperature. J Appl Polym Sci 119: 1016–1025, 2011

Key words: conducting polymers; charge transport; nanocomposites

INTRODUCTION

During the last few decades, conducting polymeric materials have been investigated extensively.[1–3] Polyaniline (PANI) is one of the best materials among this class of polymers. It has a relatively higher conductivity, a better stability, and cost effectiveness and can be easily synthesized. PANI exhibits semiconducting behavior with a relatively high conductivity because of extended π-conjugation along the polymeric backbone. Different carbon nanotubes (CNTs), such as single-walled nanotubes (SWNTs), double-walled nanotubes (DWNTs), and multiwalled nanotubes (MWNTs), also have potential applications in the fabrication of new classes of multifunctional materials because of their excellent thermal stability and mechanical and electrical properties.[4,5] When CNTs are introduced inside the polymer matrix, there is a considerable increase in the mechanical and electrical properties. This type of composite can be used in polymer-based devices. The formation of polymer–CNT networks leads to advanced materials for use in electromagnetic shielding, storage devices, electrostatic dissipation, and antennas. Hence, many efforts have been made to prepare polymer–CNT composites after Ajayan et al.[6] Not only are these composites highly stable in air, but also their electronic and physical properties change significantly. Aniline polymerizes along the CNTs, which are stabilized by strong π–π interactions between the polymer and CNTs. Hence, CNTs also align simultaneously in the polymer matrix. Many investigations reported in the literature have been done by a combination of CNTs and conducting polymers.[7–16] Wei et al.[7] studied the morphology of PANI nanotubes doped with MWNT–$(OSO_3H)_n$ and showed a one-dimensional (1D) variable range-hopping transport. Zengin et al.[8] reported the enhancement of room-temperature conductivity [σ(300 K)] in PANI–MWNT composite films. Wu et al.[10], Yan et al.,[12] and Konyushenko et al.[13] studied the conductivity change with MWNT content in the composites. Zhang and coworkers[11,14] and Long et al.[16] studied the overall temperature-dependent conductivity of PANI–MWNT composites. They also showed the negative magnetoresistance of this system. Anglada et al.[15] synthesized and characterized the SWNT-conducting polymer thin films and measured only the room-temperature resistance. Although some electrical-transport properties of conducting polymers/MWNT nanocomposites have been investigated over the last few years, it is not possible to come to any definite conclusions about their temperature- and magnetic-field-dependent electrical

Correspondence to: A. K. Meikap (meikapnitd@yahoo.com).

Contract grant sponsors: Ministry of Human Resource Development (MHRD), Government of India.

conductivity. As the trend in nanoelectronics and CNT-assisted polymeric devices increases day by day, it is necessary to have a clear idea about the electrical behavior of the PANI–CNT composites. However, major previous reports have been mainly based on the characterization of PANI–MWNT composites. The detailed study of the conductivity and magnetoconductivity of PANI–CNT composites has not been extensively explored, particularly in PANI–DWNT and PANI–SWNT below room temperature.

In this study, the fabrication and characterization of HCl doped PANI with different CNTs (SWNT, DWNT, and MWNT) was done. The low-temperature ($77 \leq T \leq 300$ K) conductivity and magnetoconductivity (up to 1 T) of these composites was investigated extensively.

EXPERIMENTAL

The composites of acid-doped PANI with CNTs was synthesized by *in situ* chemical oxidative polymerization. First, 60 mg of CNTs [SWNTs (Nanocyl 1100), DWNTs (Nanocyl 2100), or MWNTs (Nanocyl 3100)] was ultrasonicated for several hours in 300 mL of a 1*M* HCl solution in the presence of 1.136 g of cetyl trimethyl ammonium bromide to obtain a well-dispersed solution. The SWNT/HCl suspension was then preserved in a refrigerator at 1–5°C. Precooled aniline monomer (1.2 mL) and ammonium peroxydisulfate (2.72 g) dissolved in a 125-mL 1*M* HCl solution were dipped sequentially into the SWNT/HCl suspension and stirred with a magnetic stirrer. During this whole process, the temperature was maintained at 1–5°C by an ice bath. The resulting mixture was then kept in a refrigerator for 24 h. The resulting black-green suspension was filtered and washed with deionized water and methanol until the presence of cetyl trimethyl ammonium bromide and other impurities was removed. The precipitate was then dried under a dynamic vacuum for 24 h. The same procedure was used to prepare the PANI–DWNT and PANI–MWNT composites. For comparison, a pure PANI specimen was also prepared by the same technique.

Fourier transform infrared (FTIR), ultraviolet–visible (UV–vis), and photoluminescence (PL) spectroscopy were used to characterize the specimens. UV–vis spectroscopy was performed on a double-beam spectrophotometer (Hitachi, U-3010, Waltham, MA) with dimethyl sulfoxide as a solvent. PL spectroscopy was performed on a Hitachi fluorescence spectrophotometer (F-2500). FTIR was recorded on a Nicolet NEXUS FTIR spectrometer (Vernon Hills, IL) within a range of 450–4000 cm^{-1} with KBr pellets. The thermal stabilities of the samples were studied with a PerkinElmer (Waltham, MA) thermogravimetric analysis (TGA) instrument under N_2 gas. The heating rate was 10°C/min from room temperature to 900°C. X-ray intensity scans of these samples were recorded with an XPert Pro X-ray diffractometer (PANLYTICAL, Almelo, Netherlands) with nickel-filtered Cu Kα radiation ($\lambda = 1.5414$ Å) in 2θ range from 20 to 70°. Scanning electron microscopy (SEM) was used to study the morphology of the PANI–CNT composites. A very small part of the samples were dispersed in a dimethyl sulfoxide solution, and one drop of the dispersed solution was placed on a glass film. SEM was conducted at 15 kV, electronic diffraction images were recorded in a Hitachi S-300N instrument, and electronic diffraction images were recorded.

Powdered samples of the PANI, PANI–SWNT, PANI–DWNT, and PANI–MWNT composites were pressed to form pellets 1 cm in diameter under 500 MPa. To measure the electrical conductivity, standard four-probe measurements were done with good contact ensured by a highly conducting graphite adhesive (Electrodag 5513, Acheson, Williston, VT) and fine copper wires as connecting wires. Direct-current (dc) conductivity was measured by an 8½ digit Agilent 3458A multimeter. The temperature dependence of conductivity was measured in a liquid nitrogen cryostat with an ITC 502S Oxford temperature controller. We measured dc magnetoconductivity by placing the cryostat under a transverse magnetic field with variation up to 1 T by an electromagnet.

RESULTS AND DISCUSSION

The FTIR spectra of the PANI and PANI–CNT composites are shown in Figure 1. Pure PANI gave

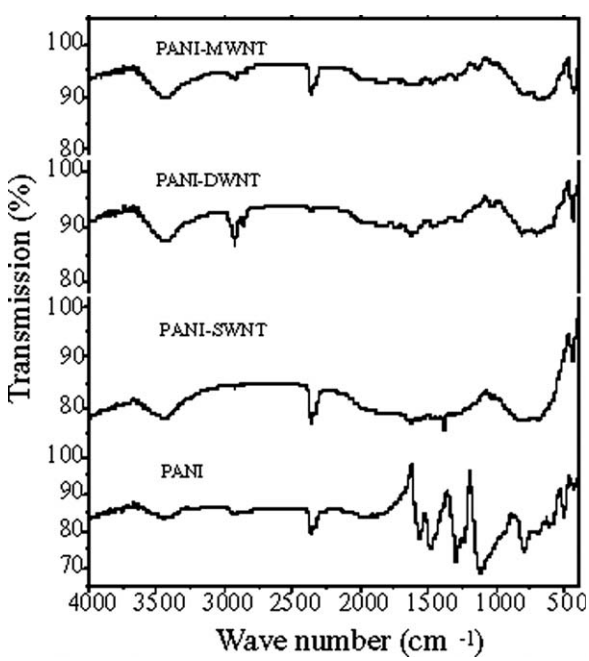

Figure 1 FTIR spectra of PANI and different PANI–CNT composites.

characteristic peaks at 3500, 2400, 1561, 1490, 1292, 1107, and 800 cm^{-1}. The peaks were attributed to the NH stretching of secondary amine, NH^+ stretching of amine, quinoid ring stretching and benzoid ring stretching, C—N stretching, vibrations of the dopant, and substitution in the benzene ring, respectively.[17] All of the peaks indicated the formation of emeraldine-base PANI. The incorporation of CNTs in the PANI matrix reduced the peak area without any shift of the peaks at 1561, 1490, 1292, 1107, and 800 cm^{-1}. This spectrum indicated that the structural change of PANI occurred with doping because of the molecular interaction of CNT with different reaction sites of PANI. Therefore, the FTIR spectrum analysis confirmed that the CNTs were embedded within the PANI matrix, which was clearer in the SEM pictures.

Figure 2 gives the scanning electron micrographs of the bare MWNT [Fig. 2(a)], PANI–SWNT [Fig. 2(b)], PANI–DWNT [Fig. 2(c)], and PANI–MWNT [Fig. 2(d)] samples, respectively. Columnar growth was been observed in the PANI–DWNT and PANI–MWNT samples; however, pellet-type growth was observed in the PANI–SWNT sample. Compared with the bare MWNTs, the diameter of the PANI–CNT composites became larger after *in situ* polymerization, which suggested that the aniline monomer was uniformly polymerized on the surface of the CNT and formed columnar and pellet-type growths. So we conformed from the SEM image that, in all of the PANI–CNT samples, the polymers were coated over the CNTs.

UV–vis spectroscopy was done to characterize the interfacial interaction between the polymer and CNTs, and the spectra are shown in Figure 3. The two characteristic absorption peaks of the samples at approximately 330 and 630–660 nm were attributable to the $\pi \rightarrow \pi^*$ transition in the benzoid ring and excitation absorption of the quinoid rings, respectively.[18,19] When the tubular nanostructure of PANI–CNT was formed, the $\pi \rightarrow \pi^*$ energy increased because of the interface of CNTs in the polymer backbone. As a result, the wavelength decreased. The lower intensity of the exciton absorption band of the quinoid rings supported the dominance of the benzoid ring. The shape of the curve depended on the carrier concentration, lifetime, and transition energy. The broad and narrow peaks were contributions of delocalized and localized charge carriers. The electrical conductivity depended on the mobility of these charge carriers.

TGA was done to investigate the thermal stability of the PANI–CNT composites. Figure 4 shows TGA thermal curves of the different composites. The mass loss of the PANI samples in the temperature range 50–110°C was mainly attributed to the loss of water molecules and the lower molecular weight oligomers from the polymer matrix. The rapid mass loss between 400 and 600°C occurred because of the oxidative degradation of the polymer in air. However,

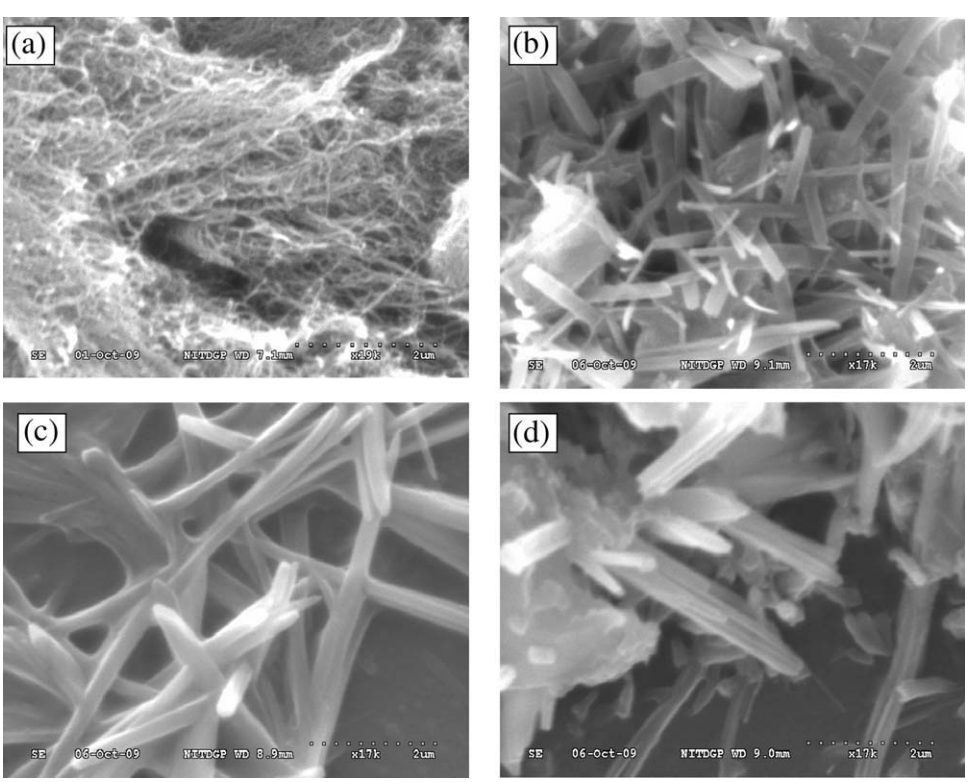

Figure 2 SEM images of (a) bare MWNT, (b) PANI–SWNT, (c) PANI–DWNT, and (d) PANI–MWNT.

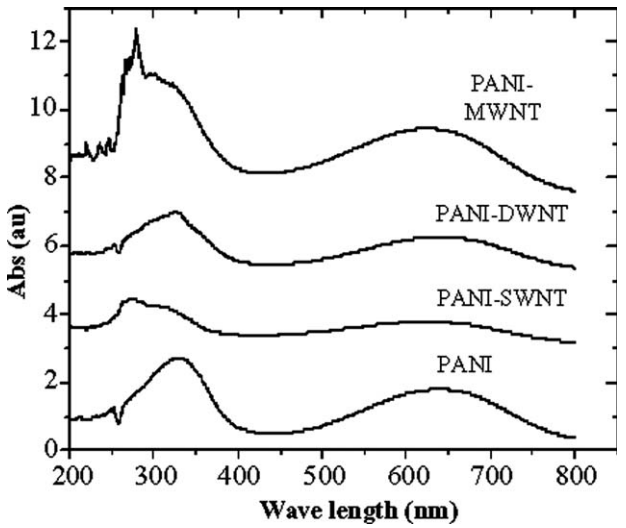

Figure 3 UV–vis spectroscopy of PANI and different PANI–CNT composites.

in the PANI–CNT composites, mass loss occurred slowly up to 600°C because of the removal of dopant molecules from the polymer structure. Rapid mass loss occurred around 600, 700, and 750°C for PANI–DWNT, PANI–SWNT, and PANI–MWNT, respectively (Table I), because of the rapid degradation of the polymer chain.[18] TGA indicated that the PANI–CNT composites were thermally more stable than PANI. We also observed that PANI–SWNT was more stable than PANI–DWNT but less stable than PANI–MWNT. Generally, the better thermal stability may have occurred because of the dominancy of the benzenoid structure over the quinoid structure in the PANI and PANI–CNT composites. Because the peak height and area of the UV–vis spectra indicated the percentage presence of the benzenoid and quinoid ring, it was clear when we compared the peak

TABLE I
Decomposition Temperature (T_d) and I_b/I_q of PANI and the PANI–CNT Composites

Sample	T_d (°C)	I_b/I_q
PANI	400	1.52
PANI–SWNT	700	1.81
PANI–DWNT	600	1.60
PANI–MWNT	750	1.99

heights of the benzenoid structure (I_b) and quinoid structure (I_q) in the UV–vis spectra, the peak at lower wavelength corresponded to the benzenoid structure, and the at higher wavelength corresponded to the quinoid structure). From the UV–vis spectra, the calculated values of the peak height ratio (I_b/I_q) were 1.52, 1.81, 1.60, and 1.99 for PANI, PANI–SWNT, PANI–DWNT, and PANI–MWNT, respectively (Table I). As the I_b/I_q of PANI was lower than that of the PANI–CNT composites, the inferior thermal stability of PANI was due to the presence of a smaller benzenoid ring in its structure compared to the PANI–CNT composite.[20] On the other hand, when we arranged the samples according to percentage presence of the benzenoid ring over the quinoid ring, it was PANI < PANI–DWNT < PANI–SWNT < PANI–MWNT. Therefore, the thermal stability, as observed in the TGA study (PANI < PANI–DWNT < PANI–SWNT < PANI–MWNT), may have been due to the presence of more benzenoid structures than quinoid structures in the PANI and different PANI–CNT composites.

The PL spectra of the PANI and PANI–CNT composites, shown in Figure 5, were determined with an excitation wavelength of 300 nm. The PANI–CNT samples showed a higher PL intensity than PANI; however, the maximum enhancement of intensity

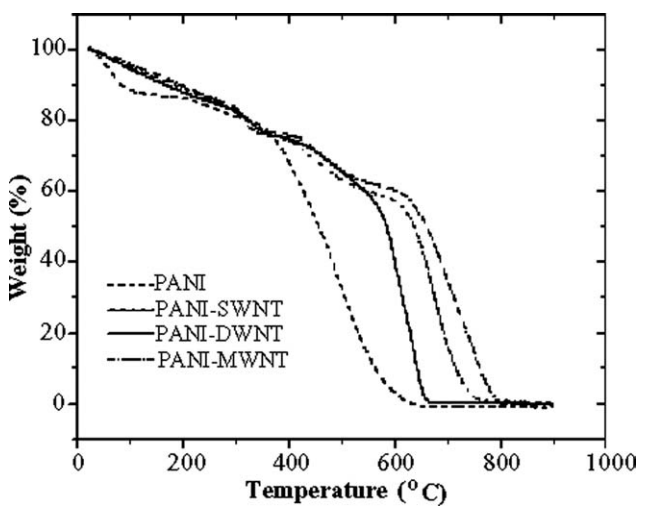

Figure 4 TGA curves of PANI and different PANI–CNT composites.

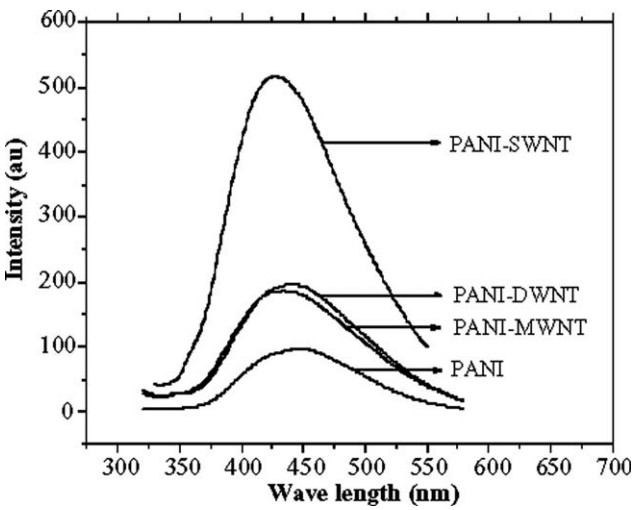

Figure 5 PL spectra of PANI and different PANI–CNT composites.

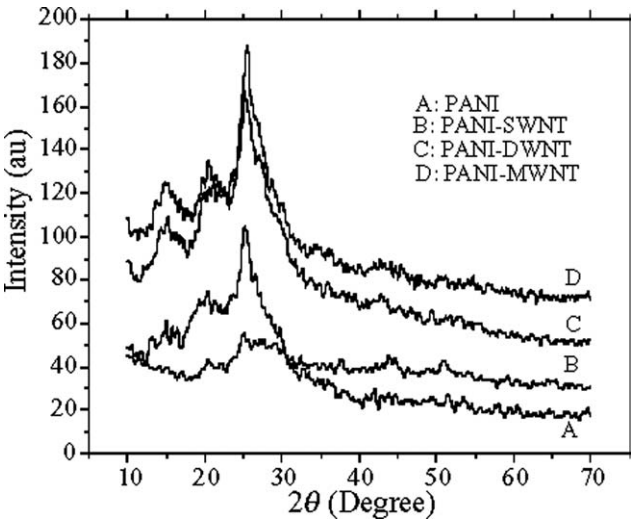

Figure 6 XRD of PANI and different PANI–CNT composites.

was observed in PANI–SWNT. It was reported that the π-bonded surface of CNTs might interact strongly with the conjugated structure of PANI, especially through the quinoid ring.[21,22] Because of this, the alignment of the polymer chain on CNTs was observed in the PANI–CNT composites,[23] which have may favored the formation of singlet excitons. This singlet exciton thus formed decays to the ground state with the emission of light. It was also observed that singlet exciton formation increased with increasing conjugation length of the polymer chain.[10] This was due to the delocalization length of the singlet exciton in the conjugated polymers, which was comparable to its conjugation length. The triplet excitons were mostly responsible for PL emission because conjugated polymers cannot produce the spin flip, which is necessary for optical transition electrons. Hence, one should expect higher PL emission from PANI–CNT composites. Emission peaks were found around 449, 427, 441, and 434 nm for PANI, PANI–SWNT, PANI–DWNT, and PANI–MWNT, respectively. We observed that the peak position shifted to the lower position for the PANI–CNT samples compared to the PANI sample, and the maximum shift (blueshift) was observed in PANI–SWNT.

Figure 6 presents the X-ray diffraction (XRD) for PANI various PANI–CNT composites. In the XRD diffractogram, PANI showed broad peaks at 2θ angles of 15° (weak), 20.4° (low intense), and 25.2°, as reported earlier.[24,25] These peaks in PANI may have arisen because of the regular repetition of the monomer unit aniline The XRD pattern of the PANI–CNT composites revealed their crystalline nature, which was similar to that of pure PANI and indicated the absence of another crystalline order. However, because of the incorporation of CNTs in PANI, the peaks were sharper, and the peak intensity increased in the composites more than in PANI prepared under the same conditions. It was reported that such behavior may arise (1) because the presence of CNTs can introduce a dopant effect on PANI and increase effective delocalization on polymer chains[8] or (2) because of the ordering of PANI macromolecules along the CNT axis.[14] Therefore, we concluded that sharper and higher peak intensities in our investigated PANI–CNT composites, compared to those in PANI, were due to the dopant effect of the CNTs and the ordering of polymer chains along the CNTs.

To form an idea of the conductivity of the PANI–CNT composites, we measured the temperature dependence of dc conductivity of the samples from 77 to 300 K. There was an increase in the σ(300 K) and the conductivity ratio [$\rho_r = \sigma(300\ K)/\sigma(77\ K)$] from 0.44 to 1.09 $\Omega^{-1}\ m^{-1}$ and from 1.39 to 3.89, respectively (Table II). As CNTs are relatively good electron acceptors and PANI can be considered a good electron donor, this enhancement may have been due to the dopant effect or charge transfer from the quinoid unit of PANI to the CNTs. Interaction between the CNTs and quinoid ring of the PANI increased the charge-transfer process between them. It was reported that the localization length (L_{loc}) of CNTs is around 10 nm for the presence of a large π-conjugated structure, whereas for crystalline and amorphous PANI, it is only around 2 nm.[26] Therefore, there would have been an enhancement of the average L_{loc} in the polymer/CNT composites. This happened because of strong coupling between the poorly conducting polymer and highly conducting CNTs. The temperature dependence of resistivity is

TABLE II
Experimentally Obtained Conductivity Parameters of PANI and the PANI–CNT Composites

			$77 \le T \le 110$ K		$110 \le T \le 300$ K	
Sample	σ(300 K) ($\Omega^{-1}\ m^{-1}$)	ρ_r	ρ(0) (Ωm)	E_a (meV)	ρ(0) (Ωm)	E_a (meV)
PANI	0.44	1.39	2.49	1.6	1.87	4.4
PANI–SWNT	0.70	3.89	2.80	4.6	0.64	19.2
PANI–DWNT	1.09	1.62	1.25	1.2	0.65	7.8
PANI–MWNT	0.58	2.26	2.71	2.5	1.07	12.4

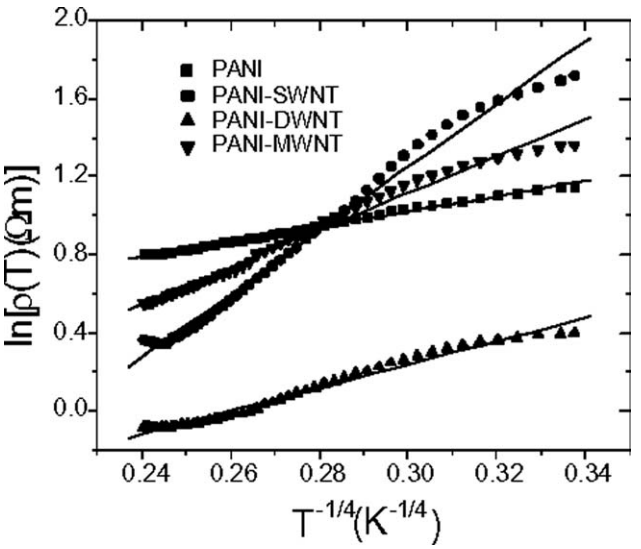

Figure 7 Temperature dependence of the dc conductivity of PANI and different PANI–CNT composites. The solid lines are fitted to eq. (1).

presented in Figure 7 for the different PANI–CNT composites. All of the samples showed semiconducting behavior; that is, their resistivity decreased with increasing temperature. This occurred because of an increase in the charge transfer between the polymer and CNTs with increasing temperature. In general, in a disordered semiconducting system, the temperature-dependent resistivity [$\rho(T)$] follows the Mott variable range-hopping model:[27]

$$\rho(T) = \rho_0 \exp\left[\left(\frac{T_{\text{Mott}}}{T}\right)^{\gamma}\right] \quad (1)$$

where ρ_0 is a constant; $T_{\text{Mott}} = \frac{24}{\pi k_B L_{\text{loc}}^3 N(E_F)}$ is the characteristic Mott temperature, which depends on the hopping barrier, electronic structure, and energy distribution of the localized states; k_B is the Boltzmann constant; L_{loc} is the localization length; $N(E_F)$ is the density of states at the Fermi level; and γ is the variable range hopping (VRH) exponent, whose value determines the dimensionality of the conducting medium by the relation $\gamma = 1/(1 + d)$, where d defines the dimensionality of the charge transport mechanism. For three-dimensional (3D), two-dimensional, and 1D systems, possible γ values are $1/4$, $1/3$, and $1/2$, respectively. To find the mechanism of the electronic-transport properties of the investigated samples, the measured dc conductivity was analyzed with the help of eq. (1). First, we have plotted a graph of $\ln[\rho(T)]$ with $T^{-1/2}$ for all of the samples (not shown in this article). The nonlinear behavior of the graph suggested that quasi-1D transport was not the dominating transport mechanism in the PANI and PANI–CNT composites. Second, we plotted a graph of $\ln[\rho(T)]$ with $T^{-1/4}$ for all of the samples, as shown in Figure 7. We observed that, for the PANI sample, a linear variation was obtained for the full investigated temperature range ($77 \leq T \leq 300$ K); however, in the case of the PANI–CNT composites, a deviation from linearity was observed at lower temperatures ($T < 180$ K). This indicated that the 3D charge-transport mechanism ($\gamma = 1/4$) was the suitable conduction mechanism for the investigated samples. Values of T_{mott} were determined from the slopes of these linear variations of $\ln[\rho(T)]$ with $T^{-1/4}$, and it was between 273 and 110,145 K for different samples. The value of T_{mott} strongly depended on the disorder present in the sample, which was measured by ρ_r, and its value increased with increasing ρ_r. Hence, the high value of T_{mott} (110,145 K) for PANI–SWNT was due to the large ρ_r ($\rho_r = 3.9$) compared to the other samples. Similar observations were obtained in many previous studies.[28,29] The value of $\gamma = 1/4$, as obtained, contradicted the results obtained by Long et al.[16] and Wang et al.[30] According to them, quasi-1D transport is the dominating transport mechanism in PANI and PANI–CNT composites. If the conducting chains are isolated, strong interchain coupling in polymer composites shows a 1D transport mechanism. However, for nonisolated conducting polymer chains, where conducting islands are present between the insulating matrix, the electronic wave functions extend in three dimensions. An SEM picture revealed that the conducting polymer chains were nonisolated and the CNTs were embedded in the PANI matrix. So, 3D VRH was the dominating charge-transport mechanism; this was supported by our experimental data. In the low-temperature range ($77 \leq T \leq 180$ K), the observed deviation from linearity in the $\ln[\rho(T)]$ versus $T^{-1/4}$ curve for the PANI–CNT composites may have been due to the dominant conduction mechanism through polymer chains, which may be clear through the study of the activation behavior of the composites. The activation behavior of the PANI–CNT composites were studied with the Arrhenius equation:

$$\rho(T) = \rho(0) \exp\left(\frac{E_a}{k_B T}\right) \quad (2)$$

where $\rho(0)$ is the resistivity at infinite temperature, E_a is the activation energy, and k_B is the Boltzmann constant. With eq. (2), E_a was calculated from the slope of the straight-line plot of $\ln[\rho(T)]$ versus $1/T$. A plot of $\ln[\rho(T)]$ with $1000/T$ is shown in Figure 8, which indicates the presence of two activation regions (two different slopes). From the slopes of the straight-line portions of the two regions, E_a's of different PANI–CNT composite samples were calculated (Table II). At low temperatures, the calculated values of E_a were 1.2 meV for PANI–DWNT, 2.5

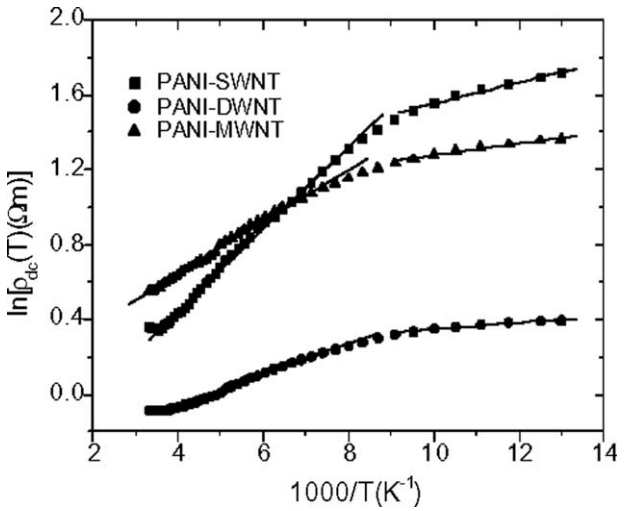

Figure 8 Variation of the dc conductivity (σ_{dc}) with temperature of different PANI–CNT composites.

meV for PANI–MWNT, and 4.6 meV for PANI–SWNT, whereas at higher temperatures, its values were 7.8 meV for PANI–DWNT, 12.4 meV for PANI–MWNT, and 19.2 meV for PANI–SWNT. As the activation behavior of PANI–CNT was closer to PANI at low temperatures than at high temperatures, it was clear that the polymer and CNT interaction was more prominent at higher temperatures than at lower temperatures. Because E_a of the CNTs was large, the strong interaction between the CNTs and conducting polymers resulted in a large E_a at higher temperatures, because of which a deviation from nonlinearity was observed in the $\ln[\rho(T)]$ versus $T^{-1/4}$ plot. Therefore, we concluded that, in the higher temperature region, charge-transport mechanisms were dominated by CNTs and polymer chains than in the lower temperature region. On the other hand, the conductivity values of all of the PANI–CNT composites were greater than that of PANI in the high-temperature range; however, the conductivities of PANI–SWNT and PANI–MWNT were lower than that of PANI. Basically, the conductivity of a material depends on the presence of disorder within the materials, which is measured by its ρ_r. We observed from the conductivity study that the values of ρ_r were 3.9 for PANI–SWNT, 2.3 for PANI–MWNT, and 1.39 for PANI. This suggested that the disorder present in PANI–SWNT and PANI–MWNT was greater than that in PANI. Therefore, at low temperatures, the lower conductivity in PANI–SWNT and PANI–MWNT in comparison to PANI may have been due to the presence of higher disorder in PANI–SWNT and PANI–MWNT. We observed from the conductivity study (Table II) that the σ(300 K) of PANI–DWNT was greater in comparison to the others; therefore, this composite would be the best electronic conductor.

The magnetic-field-dependent conductivity (magnetoconductivity) of the samples was measured within the temperature range $77 \leq T \leq 300$ K under the influence of a varying magnetic field up to 1 T. The variation of magnetoconductivity with magnetic field strength at room temperature (300 K) is shown in Figure 9. All samples showed a negative magnetoconductivity at room temperature, except PANI–SWNT, which showed a positive magnetoconductivity. The maximum percentage changes of conductivity $\left[\frac{\sigma(B,T)-\sigma(0,T)}{\sigma(0,T)} \times 100\right]$ under a magnetic field of 0.8 T at 300 K were -0.3% for PANI, -0.4% for PANI–DWNT and PANI–MWNT, and 6.5% for PANI–SWNT, where B is the magnetic field strength and σ is the conductivity. We observed that, when CNTs were incorporated into the PANI matrix, the percentage change of magnetoconductivity was nearly the same for the PANI, PANI–DWNT, and PANI–MWNT samples, but a large change was observed in PANI–SWNT compared to PANI. So we concluded that, as SWNT was incorporated into the polymer matrix, L_{loc} became higher than the other types of composites, which is explained below. The experimental data followed a simple phenomenological model consisting of two simultaneously acting hopping processes: the wave function shrinkage model[31,32] and the forward interference model.[33–35] According to the wave function shrinkage model, the wave functions of the electrons contract under a magnetic field, and the average

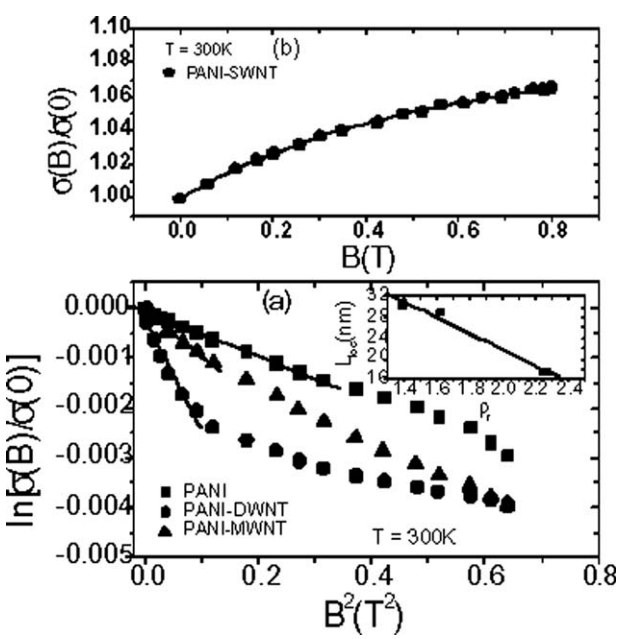

Figure 9 Variation of the dc magnetoconductivity with perpendicular magnetic field of (a) PANI, PANI–DWNT, and PANI–MWNT at 300 K [the solid lines were fitted to eq. (3)] and (b) PANI-SWNT at 300 K [the solid lines were fitted to eq. (4)].

hopping length (R_{hop}) decreases, which results in a negative magnetoconductivity; that is, the conductivity decreases with increasing magnetic field. The magnetoconductivity ratio under a small magnetic field can be written as[31]

$$\ln\left[\frac{\sigma(B,T)}{\sigma(0,T)}\right] = -t_1\frac{e^2L_{loc}^4}{\hbar^2}\left(\frac{T_{Mott}}{T}\right)^{3/4}B^2 \quad (3)$$

where $t_1 = 5/2016$ and L_{loc} is the localization length. Again, the forward interference model is about the effect of forward interference among random paths in the hopping process between two sites spaced at a distance equal to optimum hopping distance, which results in a positive magnetoconductivity. This can be expressed as

$$\frac{\sigma(B,T)}{\sigma(0,T)} = 1 + \frac{\frac{C_{sat}B}{B_{sat}}}{1+\frac{B}{B_{sat}}} \quad (4)$$

where C_{sat} is a temperature-independent parameter, B_{sat} defines the magnetic field at saturation and $B_{sat} = 0.7\left(\frac{h}{e}\right)\left(\frac{8}{3}\right)^{\frac{3}{2}}\left(\frac{1}{L_{loc}}\right)^2\left(\frac{T}{T_{Mott}}\right)^{\frac{3}{8}}$. R_{hop} is given by $R_{hop} = \left(\frac{3}{8}\right)\left(\frac{T}{T_{Mott}}\right)^{\frac{1}{4}}L_{loc}$ and becomes smaller in PANI for its small L_{loc}. Thus, the magnetoconductivity of PANI follows a wave function shrinkage model (negative magnetoconductivity), and this was widely observed in our previous studies of PANI samples.[28,29] However, a large positive magnetoconductivity was reported for CNT films and pellets at weak magnetic field because of their large L_{loc} and R_{hop} values.[36,37] This observation was interpreted in terms of the quantum interference effect. Therefore, in the PANI–CNT composites, the competition of these two (wave function shrinkage and quantum interference) contributions changed the sign and magnitude of the magnetoconductivity. As the magnetoconductivity decreased with magnetic field at 300 K for the PANI, PANI–DWNT, and PANI–MWNT samples, we assumed that the wave function shrinkage model dominated over the interference model. So, the experimental data were analyzed with the wave function shrinkage model. A plot of $\ln[\sigma(B,T)/\sigma(0,T)]$ with B^2 showed a linear variation for different samples, as shown in Figure 9. The points are the experimental results, and the curve represents the theoretical best fit in accordance with the wave function shrinkage model at low magnetic field. Figure 9 shows that experimental results were in good agreement with the theoretical model. From the slope of the curves, L_{loc} was calculated; its values were 30, 29, and 17.5 nm for PANI, PANI–DWNT, and PANI–MWNT, respectively. The variation of L_{loc} with the resistivity ratio is shown in the inset of Figure 9(a). The higher the resistivity ratio was, the higher was the disorder. Again, for high disorder, electronic wave functions are more localized within smaller regions; this results in smaller L_{loc}. Thus, there was an inverse relationship between L_{loc} and the resistivity ratio, and hence, L_{loc} depended on the disorder present in the samples, which could be characterized by the resistivity ratio (ρ_r). On the other hand, the observed positive magnetoconductivity of PANI–SWNT was analyzed with the quantum interference effect. In Figure 9(b), the points are the experimental results, and the solid line represents the theoretical best fits to eq. (4), with C_{sat} and B_{sat} as fitting parameters. We observed from the fitting that the experimental results were in good agreement with the quantum interference model. From the best-fit parameter, L_{loc} was calculated to be 43.2 nm. Hence, L_{loc} of PANI–SWNT was larger compared to that of the PANI, PANI–DWNT, and PANI–MWNT samples. R_{hop} was calculated with the following formula:

$$R_{hop} = \left(\frac{3}{8}\right)\left(\frac{T}{T_{Mott}}\right)^{\frac{1}{4}}L_{loc}$$

This yielded values of 11.1, 70.8, 19.2, and 17.1 nm for PANI, PANI–SWNT, PANI–DWNT, and PANI–MWNT, respectively. We observed that R_{hop} of PANI–SWNT was larger than the values of the other investigated samples, which was evident of a large positive magnetoconductivity in PANI–SWNT. On the other hand, the small negative magnetoconductivities of PANI, PANI–DWNT, and PANI–MWNT were due to their small R_{hop} values.

Figure 10 shows the variation of the magnetoconductivity of PANI–SWNT with various magnetic

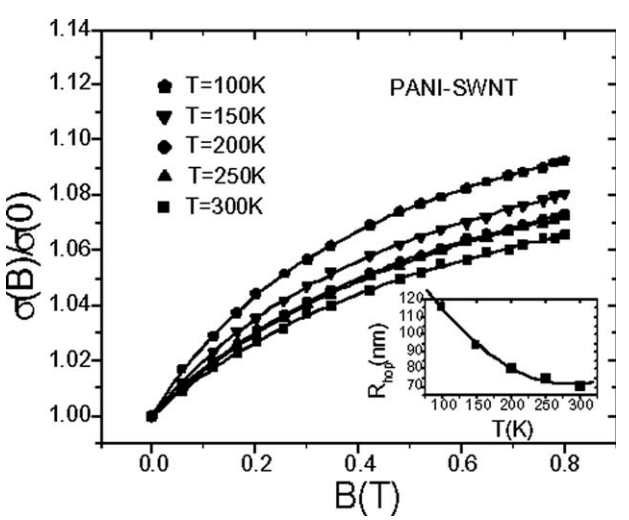

Figure 10 Variation of the dc magnetoconductivity with perpendicular magnetic field of the PANI–SWNT sample at different temperatures. The solid lines were fitted to eq. (4).

fields at different temperatures. The positive magnetoconductivity at all temperatures provided strong evidence to support the fact that the R_{hop} of the composites was enhanced and the electronic transport was dominated by SWNT. As shown in Figure 10, the experimental data were well described by the quantum interference model. From the best-fit values of the parameters, we calculated R_{hop} for different temperatures, and its variation with temperature is shown in inset of Figure 10. As the temperature decreased, the value of R_{hop} increased, so the quantum interference effect dominated over the wave function shrinkage effect, and ultimately, the magnitude of the magnetoconductivity increased with decreasing temperature.

CONCLUSIONS

PANI–CNT composites were synthesized by *in situ* chemical oxidative polymerization, and their structure, morphology, thermal stability, PL, and low-temperature conductivity were investigated. FTIR analysis revealed the formation of PANI and the change in polymer structure due to the introduction of CNTs in the polymer matrix. SEM images confirmed that, in all of the PANI–CNT samples, the polymers were coated over the CNTs. TGA provided evidence for better thermal stability in the different PANI–CNT composites. PANI–SWNT possessed the maximum PL intensity for greater chances of excitation formation; this resulted from increased π-electron mobility. UV–vis spectra supported the presence of quinoid and benzoid rings; however, the lower intensity of the exciton absorption band of the quinoid rings supported the dominance of the benzoid ring. The formation of hybrid materials was confirmed by XRD analysis. The X-ray peaks became sharper, and peak broadening occurred because of the superimposition of the peaks of the CNTs and polymers. The electrical-transport properties of the investigated samples were measured in the temperature range $77 \leq T \leq 300$ K in the presence and absence of a transverse magnetic field up to 1 T. Incorporation of CNTs in the polymer matrix increased the σ(300 K) and ρ_r. The maximum conductivity was found in the PANI–DWNT composite. So this composite may be used as the best electronic conductor. All of the composite samples had two activation processes, one due to a dominant charge-transfer process by PANI at lower temperatures and the other due to PANI–CNT composites at higher temperatures. Negative magnetoconductivities were observed in PANI and the PANI–DWNT and PANI–MWNT composites, which was explained by the wave function shrinkage model, whereas the positive magnetoconductivity of PANI–SWNT was interpreted by the quantum interference effect. R_{hop} increased from 70.8 to 116.0 nm with decreasing temperature from 300 to 100 K for PANI–SWNT.

One of the authors (A.K.M.) is thankful to Technical Education Quality Improvement Programme (TEQIP), Government of India, for providing financial assistance to visit the University of Dublin, Ireland.

References

1. Naarman, H. Science and Application of Conducting Polymers; Hilger: Bristol, United Kingdom, 1991.
2. Seanor, D. A. Electronic Properties of Polymers; Academic: New York, 1992.
3. MacDiarmid, A. G. Conjugated Polymers and Related Materials; Oxford University Press: London, 1993.
4. Mintmire, J. W.; Dunlop, B. I.; Carter, C. T. Phys Rev Lett 1992, 73, 2468.
5. Overney, G.; Zhong, W.; Tomanek, T. Z Phys D 1993, 27, 93.
6. Ajayan, P. M.; Stephan, O.; Colliex, C.; Trauth, D. Science 1993, 365, 1212.
7. Wei, Z.; Wan, M.; Lin, T.; Dai, L. Adv Mater 2003, 15, 136.
8. Zengin, H.; Zhou, W.; Jin, J.; Czerw, R.; Smith, D. W., Jr.; Echegoyen, L.; Carroll, D. L.; Foulger, S. H.; Ballato, J. Adv Mater 2002, 14, 1480.
9. Blanchet, G. B.; Fincher, C. R.; Gao, F. Appl Phys Lett 2003, 82, 1290.
10. Wu, T. M.; Lin, Y. W.; Liao, C. S. Carbon 2005, 43, 734.
11. Zhang, X.; Zhang, J.; Wang, R.; Liu, Z. Carbon 2004, 42, 1455.
12. Yan, X.; Han, Z. J.; Yang, Y.; Tay, B. K. J Phys Chem C 2007, 111, 4125.
13. Konyushenko, E. N.; Stejskal, J.; Trchova, M.; Hradil, J.; Kovarova, J.; Prokes, J.; Cieslar, M.; Hwang, J. Y.; Chen, K. H.; Sapurina, I. Polymer 2006, 47, 5715.
14. Zhang, X.; Zhang, J.; Liu, Z. Appl Phys A 2005, 80, 1813.
15. Anglada, N. F.; Kaempgen, M.; Skakalova, V.; Weglikowska, U. D.; Roth, S.; Diamond Relat Mater 2004, 13, 256.
16. Long, Y.; Chen, Z.; Zhang, X.; Zhang, J, Liu, Z. Appl Phys Lett 2004, 85, 1796.
17. Amrithesh, M.; Aravind, S.; Jayalekshmi, S.; Jayasree, R. S. J Alloys Compd 2008, 449, 176.
18. Erdem, E.; Karakisla, M.; Sacak, M. Eur Polym J 2004, 40, 785.
19. Ding, S.; Mao, H.; Zhang, W. J Appl Polym Sci 2008, 109, 2842.
20. Sarkar, A.; Ghosh, P.; Meikap, A. K.; Chattopadhyay, S. K.; Chatterjee, S. K.; Choudhury, P.; Roy, K.; Saha, B. J Appl Polym Sci 2008, 108, 2312.
21. Quillard, S.; Louarn, G.; Lefrant, S.; MacDiarmid, A. G. Phys Rev B 1994, 50, 12496.
22. Chen, R. J.; Zhang, Y.; Wang, D.; Dai, H. J Am Chem Soc 2001, 123, 3838.
23. Feng, W.; Bai, X. D.; Lian, Y. Q.; Liang, J.; Wang, X. G.; Yoshino, K. Carbon 2003, 41, 1551.
24. Wise, D. L.; Wnek, G. E.; Trantlolo, D.; Cooper, T. M.; Gresser, J. D. Photonic Polymer Systems—Fundamentals, Methods and Applications; Marcel Dekker: New York, 1998.
25. Chaudhari, H. K.; Kelkar, D. S. Polym Int 1997, 42, 380.
26. Joo, J.; Long, S. M.; Pouget, J. P.; Oh, E. J.; MacDiarmid, A. G.; Epstein, A. J. Phys Rev B 1998, 57, 9567.
27. Mott, N. F.; Davis, E. Electronic Process in Noncrystalline Materials; 2nd ed.; Clarendon: Oxford, 1979.

28. Ghosh, M.; Barman, A.; Meikap, A. K.; De, S. K.; Chatterjee, S. Phys Lett A 1999, 260, 138.
29. Ghosh, P.; Sarkar, A.; Meikap, A. K.; Chattopadhyay, S. K.; Chatterjee, S. K.; Ghosh, M. J Phys D: Appl Phys 2006, 39, 3047.
30. Wang, Z. H.; Scherr, E. M.; MacDiarmid, A. G.; Epstein, A. J. Phys Rev B 1992, 45, 4190.
31. Shklovskii, B. I. Sov Phys Semicond 1983 17, 1311.
32. Shklovskii, B. I.; Efros, A. L. Electronic Properties of Doped Semiconductors; Springer: Berlin, 1984; p 202.
33. Nguyen, V. L.; Spivak, B. Z.; Shklovskii, B. I. Sov Phys JETP 1995, 62, 1021.
34. Sivan, U.; Entin-Wohiman, O.; Imry, Y. Phys Rev Lett 1988, 60, 1566.
35. Rosenbaum, R.; Milner, A.; Hannens, S.; Murphy, T.; Palm, E.; Brandt, B. Phys B 2001, 294–295, 340.
36. Fuhrer, M. S.; Holmes, W.; Richards, P. L.; Delaney, P.; Louie, S. G.; Zettl, A. Synth Met 1999, 103, 2529.
37. Yosida, Y.; Oguro, I. J Appl Phys 1999, 86, 999.